Article

Single-photon nonlinearity at room temperature

https://doi.org/10.1038/s41586-021-03866-9

Received: 25 December 2020

Accepted: 29 July 2021

Published online: 22 September 2021

Check for updates

Anton V. Zasedatelev[1,2]✉, Anton V. Baranikov[1,2], Denis Sannikov[1,2], Darius Urbonas[3], Fabio Scafirimuto[3], Vladislav Yu. Shishkov[1,2,4,5], Evgeny S. Andrianov[1,2,4,5], Yurii E. Lozovik[1,2,4,6,7], Ullrich Scherf[8], Thilo Stöferle[3], Rainer F. Mahrt[3] & Pavlos G. Lagoudakis[1,2,9]✉

The recent progress in nanotechnology[1,2] and single-molecule spectroscopy[3–5] paves the way for emergent cost-effective organic quantum optical technologies with potential applications in useful devices operating at ambient conditions. We harness a π-conjugated ladder-type polymer strongly coupled to a microcavity forming hybrid light–matter states, so-called exciton-polaritons, to create exciton-polariton condensates with quantum fluid properties. Obeying Bose statistics, exciton-polaritons exhibit an extreme nonlinearity when undergoing bosonic stimulation[6], which we have managed to trigger at the single-photon level, thereby providing an efficient way for all-optical ultrafast control over the macroscopic condensate wavefunction. Here, we utilize stable excitons dressed with high-energy molecular vibrations, allowing for single-photon nonlinear operation at ambient conditions. This opens new horizons for practical implementations like sub-picosecond switching, amplification and all-optical logic at the fundamental quantum limit.

Nonlinear optical phenomena are at heart of diverse applications ranging from telecommunication to data storage, high-resolution microscopy, and lithography, among others. In photonics, the implementation of nonlinear effects at the single-photon level is highly desirable as it can drive power consumption of all-optical switches, optical modulators and optical transistors to their fundamental limit. Furthermore, single-photon nonlinearities offer unique applications for optical quantum control and new paradigms for optical computing, optical communications and metrology[7,8]. Considerable efforts are invested in the achievement of single-photon nonlinearity across a plethora of material systems and physical principles. Platforms range from a single atom[9–12], including artificial solid-state atoms[13–16] coupled to a high-finesse cavity probing the nonlinear regime of cavity quantum electrodynamics (cQED) to ultracold atomic ensembles[17–19]. Unlike their single-emitter counterparts, the ultracold atomic ensembles probed the single-photon nonlinearity by means of quantum interference in strongly correlated many-body systems. These systems are more robust and scalable, but sophisticated cooling and quantum-state preparation techniques, alongside high-vacuum and cryogenic conditions, compromise their use substantially.

Strong coupling of semiconductor materials in optical microcavities can potentially combine the above concepts of cQED and correlated many-body physics to give rise to hybrid light–matter states that are much more robust to high temperatures[20]. Obeying Bose statistics and despite their non-equilibrium nature, under certain conditions exciton-polaritons undergo a transition to a macroscopically occupied state exhibiting off-diagonal long-range order[21–23]. The coherent and nonlinear nature of polariton condensates[24] makes them outstanding candidates for integrated on-chip photonics[6,25,26]. Here, we demonstrate ultrafast single-photon optical switching and amplification operational at ambient conditions, using a π-conjugated ladder-type polymer strongly coupled to an optical microcavity.

Polariton condensation via vibrations

Hereafter, we employ an organic semiconductor polymer microcavity consisting of a 35-nm-thick film of π-conjugated ladder-type polymer called MeLPPP, encapsulated by 50 nm SiO_2 spacers on either side sandwiched between SiO_2/Ta_2O_5-distributed Bragg reflectors (DBR) constituting a $\lambda/2$ optical microcavity (see Methods). The structure design and related properties in the strong light–matter interaction regime have been extensively studied in refs. [6,23,27], and in the Supplementary Section I we provide further spectroscopic evidence of strong coupling. To minimize heating of the molecules, we pump the uncoupled exciton reservoir resonantly at the exciton transition using 150 fs pulses, and optimize the incident angle of the pump beam to minimize reflection losses, as shown schematically in Fig. 1a. Exciton energy relaxation populates polariton states predominantly through intracavity radiative pumping and vibron-assisted thermalization[28–30]. Recently, we demonstrated that in the presence of strong vibrational resonances in organic microcavities, a single-step exciton–vibron scattering can efficiently populate the lower polariton dispersion[6]. Therefore, we choose the detuning of the exciton–photon resonance to satisfy the

[1]Center for Photonics and Quantum Materials, Skolkovo Institute of Science and Technology, Moscow, Russia. [2]Laboratories for Hybrid Photonics, Skolkovo Institute of Science and Technology, Moscow, Russia. [3]IBM Research Europe - Zurich, Rüschlikon, Switzerland. [4]Dukhov Research Institute of Automatics (VNIIA), Moscow, Russia. [5]Moscow Institute of Physics and Technology, Dolgoprudny, Russia. [6]Institute for Spectroscopy RAS, Troitsk, Russia. [7]Moscow Institute of Electronics and Mathematics, National Research University Higher School of Economics, Moscow, Russia. [8]Macromolecular Chemistry Group and Institute for Polymer Technology, Bergische Universität Wuppertal, Wuppertal, Germany. [9]Department of Physics and Astronomy, University of Southampton, Southampton, UK. ✉e-mail: a.zasedatelev@skoltech.ru; p.lagoudakis@skoltech.ru

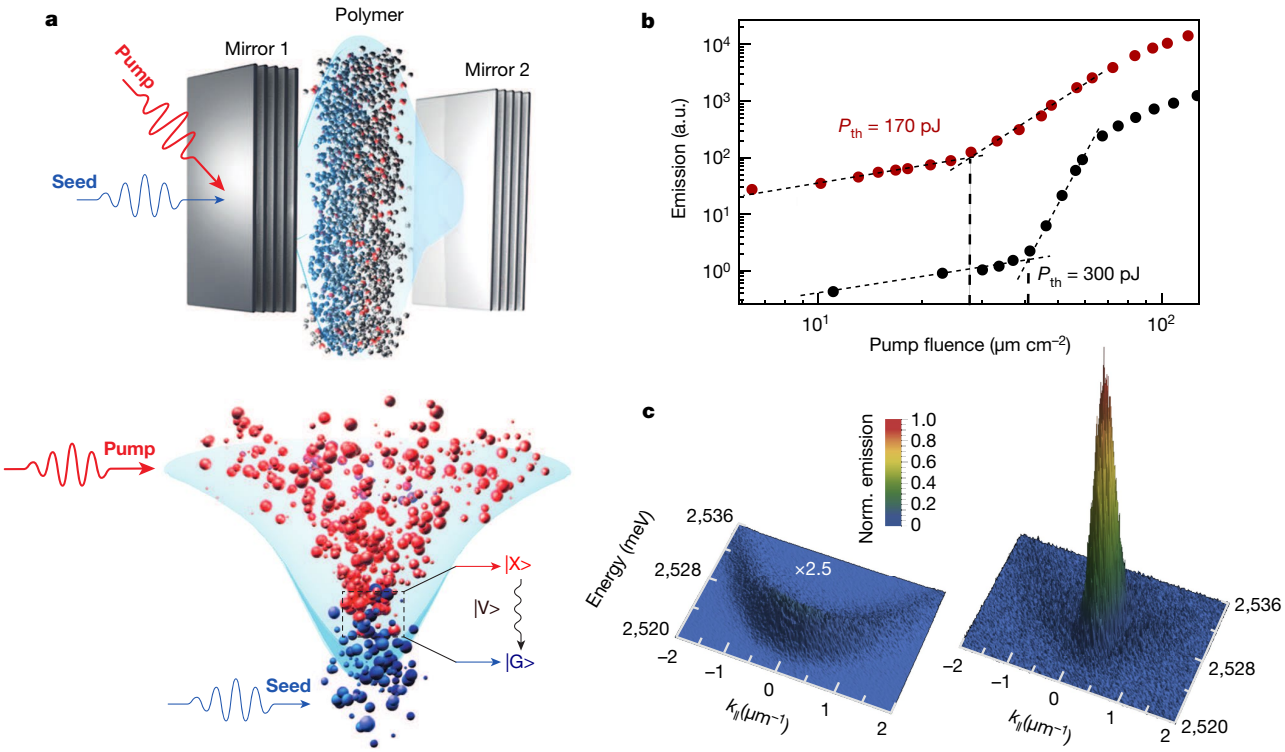

Fig. 1 | The principle of the extreme nonlinearity in organics. a, The schematic illustrates the principle of stimulated relaxation from the exciton reservoir (X) towards the ground polariton state (G) via molecular vibron (V). **b**, Integrated emission as a function of pump fluence plotted for the spontaneously formed (black dots) and seeded (red dots) polariton condensates at a pump energy threshold of 300 pJ and 170 pJ, respectively, shown by vertical dashed lines. **c**, Energy–momentum *(E, k)* distribution for spontaneously formed (left) and seeded (right) polariton condensates respectively. Incident pump fluence is 80 μJ cm^{-2} ($P \approx 2P_{th}$), energy of the seed beam is 460 aJ.

following condition: $\hbar\omega_{exc} = \hbar\omega_{pol} + \hbar\omega_{vib}$, between the exciton reservoir ($\hbar\omega_{exc}$) and the ground polariton state ($\hbar\omega_{pol}$), where $\hbar\omega_{vib}$ is the energy of the molecular vibron. By optimizing the pump and detuning conditions as described above, we achieve a polariton condensation threshold at an absorbed fluence of $P_{th} \approx 8$ μJ cm^{-2}, that is, 300 pJ incident pump pulse energy (see Methods), among the lowest values reported across all different types of strongly coupled organic semiconductor microcavities; for comparison see Supplementary Section II. Figure 1b shows the pump fluence dependence of the emission intensity from the ground polariton state, where a superlinear increase above threshold is observed, indicating the transition to polariton condensation. We corroborated the transition to a polariton condensate through a full analysis of the redistribution of polaritons along the lower polariton dispersion, which exhibit a collapse of the polariton wavefunction at the ground polariton state, and a concomitant narrowing of the spectral linewidth and energy blueshift at threshold pump fluence (see Supplementary Section II).

The principle of on-demand condensation

In the following, we utilize the effectiveness of the exciton–vibron relaxation process that underpins the low polariton condensation threshold reported here, to trigger bosonic stimulation and amplify a seed pulse resonant to the ground polariton state, as shown in Fig. 1a (see Methods). To maximize the efficiency of stimulation towards the ground polariton state we optimize both the spatial and temporal overlap between the seed and pump beams. Finally, we attenuate the seed down to the level of 460 aJ per pulse corresponding to ~1,140 polaritons resonantly injected directly into the ground state. Seeding the ground polariton state drastically increases the exciton-to-polariton relaxation rate, allowing for polariton condensation at half the exciton reservoir density and boosting the state's occupancy. According to the pump fluence dependence presented in Fig. 1b, resonant seeding results in ~50 times higher integrated emission compared to the spontaneously formed condensate. The stimulation effect on energy–momentum (E, k) distributions of the condensate is shown in Fig. 1c (see Methods).

Further on, we investigate the control over the condensate occupancy by harnessing progressively smaller seed energy as shown in Fig. 2a–c. With decreasing seed energy we observe a substantial reduction of the ground-state population, although even at the lowest seed energy of 1 aJ, carrying on average only 2.5 photons per pulse, we are still able to resolve an increase in the condensate population. Figure 2d shows emission spectra obtained from integrated E, k distributions over a momentum range of ±0.2 μm^{-1}, exhibiting a clear photoluminescence increase of the seeded (coloured lines) versus spontaneously formed condensates (black line). Comparing the spectral area in Fig. 2d we detect nearly 55% difference in the ground state population for the case of 1 aJ seed energy. To minimize fluctuations of the condensate occupation number caused by the pump-induced exciton reservoir density variations, we excite the system close to the gain saturation regime at $2P_{th}$ and integrate the output signal over 5,000 single-shot condensate realizations on the detector (see Methods).

Optical switching by sub-attojoule seed

We quantify the increase in the condensate occupancy on the average number of photons in the seed pulse by defining the contrast as a figure of merit parameter depending on the ratio of integrated population at the ground state between spontaneously formed (P_{spont}) and seeded polariton condensates (P_{seed}): Contrast $= \frac{P_{seed}}{P_{spont}} - 1$. This contrast reveals

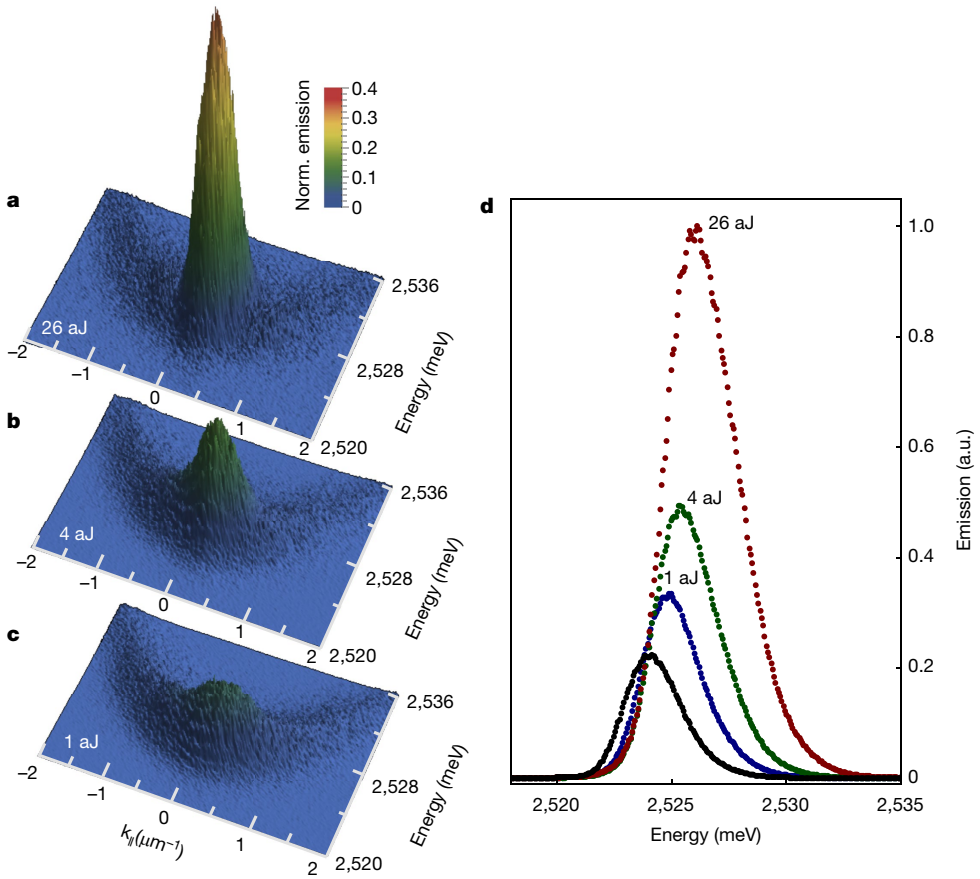

Fig. 2 | Attojoule polariton switch. a–**c**, Energy–momentum *(E, k)* distributions of 5,000 integrated condensate realizations, seeded with 26 aJ (**a**), 4 aJ (**b**) and 1 aJ (**c**) pulses. **d**, Emission spectra obtained from *(E, k)* distributions in **a**–**c** by integrating over ±0.2 μm^{-1} in momentum space. Red, green and blue dots correspond to the polariton condensate seeded with 26 aJ, 4 aJ and 1 aJ pulses, respectively, while black dots display the emission spectrum of spontaneously formed polariton condensates without seed.

a nearly power-law dependence on the average photon number of the seed, shown in Fig. 3. We experimentally observe the onset of condensation triggered by seed pulses carrying ~1.5 photons on average, with a probability larger than 0.95. Figure 3 shows that for the lowest energy seed pulses, the 2σ error bar clearly exceeds the 0% contrast level of spontaneously formed condensates. To describe the switching process we have developed a multi-mode microscopic theory of the seeded vibron-mediated polariton condensation (see Supplementary Section III). Numerical simulations are in a good agreement with the experimentally observed contrast dependence, as shown in Fig. 3 (solid curve), integrated over ±0.2 μm^{-1} in momentum space. Notably, the microscopic theory predicts a contrast of ~28% at the single-photon level; an in-depth analysis of the mechanisms underpinning the observed nonlinearity is presented in Supplementary Sections IV and V.

Despite the agreement between our experimental observation and the microscopic theory, when approaching the single-photon regime with a light source that obeys a Poissonian photon number distribution, the statistical properties of the source can no longer be neglected. In the few-photon regime, the tail of the distribution containing higher photon number states can significantly contribute to polariton stimulation; the probability of having n photons in the distribution scales with its maximum at $\langle n \rangle$ average photons as $\frac{\langle n \rangle !}{n!}\langle n \rangle^{n-\langle n \rangle}$. For example, for a seed pulse with four photons on average, instances of ten-photon events occur with ~37 times lower probability than four-photon events. Therefore, at the few-photon regime, integrated measurements of the photoluminescence intensity over thousands of seed pulses may be skewed by higher photon number states.

Single-photon nonlinearity in single shots

To address this conundrum, we implement a single-shot measurement technique, using the same pump–seed excitation geometry, while allowing for pulse-to-pulse analysis of the condensate population,

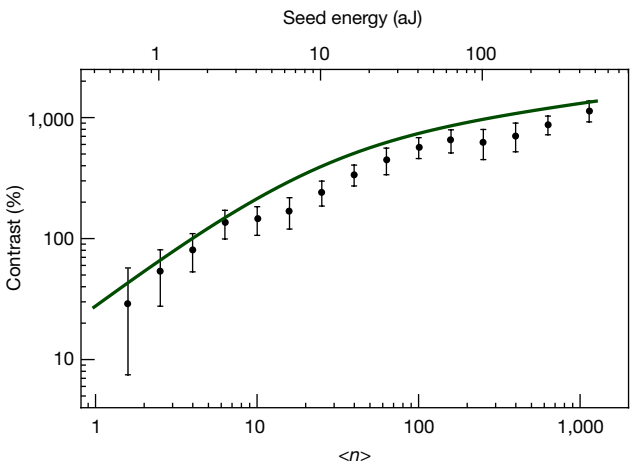

Fig. 3 | Polariton switching contrast towards the single-photon level. The contrast in population between seeded and spontaneously formed polariton condensates as the function of seed energy (top axis) and average photon number per pulse (bottom axis). Solid curve shows the result of numerical simulations of the microscopic theoretical model. The error bars show 2σ (95.4%) confidence intervals of the switching contrast.

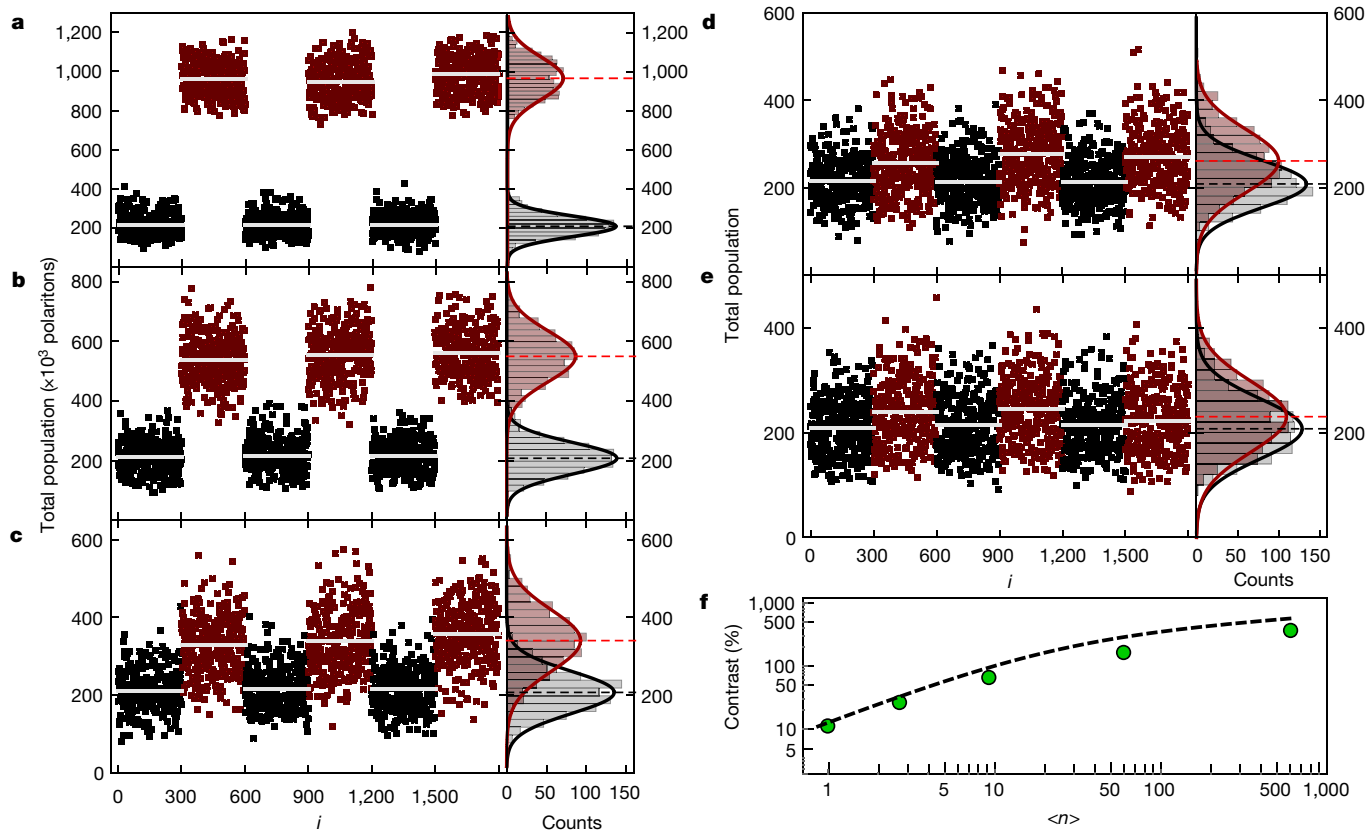

Fig. 4 | Single-photon switching for single-shot condensate realizations. **a**–**e**, Total polariton populations recorded within ±1 μm^{-1} wavevector range in the single-shot regime for a sequence of 300-to-300 spontaneously formed (black dots) and seeded (red dots) polariton condensate realizations (*i*). Seeded realizations are triggered by ⟨*n*⟩ equals 600, 60, 9.3, 2.7 and 1 photon per pulse on average as shown in **a**–**e**, respectively. Right panels represent histograms of total polariton population within single-shot condensate realizations seeded with the respective ⟨*n*⟩ photon number state (red) as well as histograms of the spontaneously formed condensates (black), both fitted by Gaussian distributions. **f**, Switching contrast versus average number of photons ⟨*n*⟩ per seed pulse obtained from statistical analysis of the histograms. The dashed curve shows the result of numerical simulations of the microscopic theoretical model.

and record the photoluminescence in real space, using appropriate filtering in momentum space (within ±1 μm^{-1}; see Methods). We seed the ground state for 300 sequentially recorded pulses, and then we switch the seed beam off allowing for 300 successive realizations of spontaneously formed polariton condensates and repeat the whole sequence three consecutive times, as shown in Fig. 4a–e. Single-shot condensate realizations, in the presence/absence of seed pulses containing ⟨*n*⟩ = 600, 60, 9.3, 2.7 and 1 photon per pulse, reveal a contrast with an average value of about 350%, 160%, 60%, 25% and 11%, respectively. The right panels of Fig. 4a–e show histograms of the polariton population for each spontaneously formed (black) and seeded (red) condensate realizations fitted by Gaussian distributions. The Gaussian fit is justified by a large number of polaritons in the condensate exhibiting excessive noise in the total polariton number. A relatively large noise is most likely to be the result of dynamic spatial disorder of the condensate[31,32], which is transformed to the disorder in the momentum space. Shot-to-shot fluctuations of the condensate in the momentum space lead to the excessive intensity noise in our detection scheme as the momentum-filter is used (see Supplementary Section VI). Therefore, the contrast-to-noise ratio in this case is not limited by any fundamental reason and, in principle, can be improved substantially by means of engineering the filter bandwidth, size of the condensate, pump fluence, configuration of seeded states and so on. As the experimental distributions are well-approximated by Gaussian distributions, our statistical analysis yields almost the same mean contrast values of 360%, 160%, 63%, 26% and 11%, as shown in Fig. 4f. We note that the results obtained from single-shot condensate realizations show a lower contrast at the single-photon regime, with respect to the integrated measurements of Fig. 3, that is, 11% versus 20–30%, while exhibiting the theoretically predicted power-law contrast dependence on ⟨*n*⟩ integrated over ±1 μm^{-1} in momentum space.

In conclusion, we report experimental evidence of single-photon nonlinearity in organic polariton condensates, underpinned by bosonic stimulation of exciton-polaritons to the ground polariton state. Our investigation demonstrates few-photon control over the polariton condensate occupancy with a record amplification of ~23,000 polaritons for every resonantly injected polariton. At the single average photon level, we observe all-optical polariton switching with a contrast of ~20–30% as shown by time-integrated measurements, and ~11% following a pulse-to-pulse analysis of single-shot condensate realizations. The rapid progress of organic polaritonics has opened new routes for all-optical switching and logic at ambient conditions[6,27]. Our investigation here takes these applications to the single-photon level, thereby bridging quantum properties of light with classical phenomena of massively occupied states of light–matter Bose–Einstein condensates.

Online content

Any methods, additional references, Nature Research reporting summaries, source data, extended data, supplementary information, acknowledgements, peer review information; details of author contributions and competing interests; and statements of data and code availability are available at https://doi.org/10.1038/s41586-021-03866-9.

1. Chikkaraddy, R. et al. Single-molecule strong coupling at room temperature in plasmonic nanocavities. *Nature* **535**, 127–130 (2016).
2. Hail, C. U. et al. Nanoprinting organic molecules at the quantum level. *Nat. Commun.* **10**, 1880 (2019).
3. Maser, A., Gmeiner, B., Utikal, T., Götzinger, S. & Sandoghdar, V. Few-photon coherent nonlinear optics with a single molecule. *Nat. Photon.* **10**, 450–453 (2016).
4. Wang, D. et al. Coherent coupling of a single molecule to a scanning Fabry-Perot microcavity. *Phys. Rev. X* **7**, 021014 (2017).
5. Wang, D. et al. Turning a molecule into a coherent two-level quantum system. *Nat. Phys.* **15**, 483–489 (2019).
6. Zasedatelev, A. V. et al. A room-temperature organic polariton transistor. *Nat. Photon.* **13**, 378–383 (2019).
7. Walmsley, I. A. Quantum optics: science and technology in a new light. *Science* **348**, 525–530 (2015).
8. Chang, D. E., Vuletić, V. & Lukin, M. D. Quantum nonlinear optics—photon by photon. *Nat. Photon.* **6**, 685–694 (2014).
9. Reiserer, A., Ritter, S. & Rempe, G. Nondestructive detection of an optical photon. *Science* **342**, 1349–1351 (2013).
10. Shomroni, I. et al. All-optical routing of single photons by a one-atom switch controlled by a single photon. *Science* **346**, 903–906 (2014).
11. Tiecke, T. G. et al. Nanophotonic quantum phase switch with a single atom. *Nature* **508**, 241–244 (2014).
12. Hacker, B., Welte, S., Rempe, S. & Ritter, S. A photon–photon quantum gate based on a single atom in an optical resonator. *Nature* **536**, 193–196 (2016).
13. Volz, T. et al. Ultrafast all-optical switching by single photons. *Nat. Photon.* **6**, 605–609 (2012).
14. Giesz, V. et al. Coherent manipulation of a solid-state artificial atom with few photons. *Nat. Commun.* **7**, 11986 (2016).
15. Sun, S., Kim, H., Luo, Z., Solomon, G. S. & Waks, E. A single-photon switch and transistor enabled by a solid-state quantum memory. *Science* **361**, 57–60 (2018).
16. Dietrich, C. P., Fiore, A., Thompson, M. G., Kamp, M. & Höfling, S. GaAs integrated quantum photonics: towards compact and multi-functional quantum photonic integrated circuits. *Laser Photon. Rev.* **10**, 870–894 (2016).
17. Peyronel, T. et al. Quantum nonlinear optics with single photons enabled by strongly interacting atoms. *Nature* **488**, 57–60 (2012).
18. Chen, W. et al. All-optical switch and transistor gated by one stored photon. *Science* **341**, 768–770 (2013).
19. Gorniaczyk, H., Tresp, C., Schmidt, J., Fedder, H. & Hofferberth, S. Single-photon transistor mediated by interstate Rydberg interactions. *Phys. Rev. Lett.* **113**, 053601 (2014).
20. Sanvitto, D. & Kéna-Cohen, S. The road towards polaritonic devices. *Nat. Mater.* **15**, 1061–1073 (2016).
21. Deng, H., Haug, H. & Yamamoto, Y. Exciton-polariton Bose-Einstein condensation. *Rev. Mod. Phys.* **82**, 1489–1537 (2010).
22. Kasprzak, J. et al. Bose–Einstein condensation of exciton polaritons. *Nature* **443**, 409–414 (2006).
23. Plumhof, J. D., Stöferle, T., Mai, L., Scherf, U. & Mahrt, R. F. Room-temperature Bose–Einstein condensation of cavity exciton–polaritons in a polymer. *Nat. Mater.* **13**, 247–252 (2014).
24. Carusotto, I. & Ciuti, C. Quantum fluids of light. *Rev. Mod. Phys.* **85**, 299–366 (2013).
25. Lerario, G. et al. Room-temperature superfluidity in a polariton condensate. *Nat. Phys.* **13**, 837–841 (2017).
26. Sun, Z. & Snoke, D. W. Optical switching with organics. *Nat. Photon.* **13**, 370–371 (2019).
27. Baranikov, A. V. et al. All-optical cascadable universal logic gate with sub-picosecond operation. Preprint at https://arxiv.org/abs/2005.04802 (2020).
28. Tartakovskii, A. I. et al. Raman scattering in strongly coupled organic semiconductor microcavities. *Phys. Rev. B* **63**, 121302 (2001).
29. Coles, D. M. et al. Vibrationally assisted polariton-relaxation processes in strongly coupled organic-semiconductor microcavities. *Adv. Funct. Mater.* **21**, 3691–3696 (2011).
30. Grant, R. T. et al. Efficient radiative pumping of polaritons in a strongly coupled microcavity by a fluorescent molecular dye. *Adv. Opt. Mater.* **4**, 1615–1623 (2016).
31. Daskalakis, K. S., Maier, S. A. & Kéna-Cohen, S. Spatial coherence and stability in a disordered organic polariton condensate. *Phys. Rev. Lett.* **115**, 035301 (2015).
32. Bobrovska, N. et al. Dynamical instability of a nonequilibrium exciton-polariton condensate. *ACS Photon.* **5**, 111–118 (2018).

Methods

Sample fabrication

The sample is composed of a bottom distributed Bragg reflector (DBR) on a fused silica substrate (mirror 2), a central cavity defect region with an effective thickness slightly larger than half the exciton transition wavelength, and a top DBR (mirror 1). The DBRs consist of alternating SiO_2/Ta_2O_5 quarter-wavelength-thick layers produced by sputter deposition (9 + 0.5 pairs for the bottom DBR, 6 + 0.5 for the top DBR). The centre of the cavity consists of the polymer layer sandwiched between 50 nm spacer layers of sputtered SiO_2. The SiO_2 spacer is sputtered on the organic using a SiO_2 sputter target. Methyl-substituted ladder-type poly(p-phenylene) (MeLPPP; M_n = 31,500 (number averaged molecular weight), M_w = 79,000 (weight averaged molecular weight)) was synthesized as described elsewhere[33]. MeLPPP is dissolved in toluene and spin-coated on the bottom spacer layer. The film thickness of approximately 35 nm is measured with a profilometer (Veeco Dektak).

Spectroscopy

The pump beam with 150–200 fs pulse duration was generated by a tunable optical parametric amplifier (Coherent OPerA SOLO), which was pumped by 500 Hz high-energy Ti:sapphire regenerative amplifier (Coherent Libra-HE). The centre wavelength was adjusted with respect to experiments at 2.72 eV with 30 meV full width at half maximum (FWHM). The angle of incidence to the sample was 45°. The pulses were focused at the sample to a 20 μm × 32 μm Gaussian spot at FWHM. We measured the reflectance of the beam at 45° of incidence (R = 0.81). Since the transmitted light through the sample is negligible and strongly dependent on scattering from defects, we assumed that it is all absorbed by the structure ($1 - R$ = 0.19), thus providing an upper boundary of the absorbed fluence. Therefore, the given incident fluence of 42 μJ cm^{-2} at the threshold of the spontaneously formed condensate becomes 8 μJ cm^{-2} in terms of the absorbed value.

Filtered broadband white-light continuum (WLC) generated in a sapphire plate with photon energies in the range 2.45–2.6 eV was utilized as the seed beam with 150–250 fs pulse duration. The seed beam was focused on the sample at the normal incidence to 5 μm spot size with a microscope objective (10× Nikon, numerical aperture (NA) = 0.3), which allows the seeding of the ground polariton state within a wavevector range of ±0.2 μm^{-1}. The energy of the seed beam is defined as the incident pulse within the full linewidth of the seeded state (that is, before sample). In all measurements, temporal and spatial overlap between the control and the pump beams were optimized by maximizing the signal of the output nonlinear emission from the sample. Temporal overlap was varied by using a motorized translation stage with retroreflector in the seed beam optical path.

Integrated energy–momentum E, k distributions were acquired in transmission geometry. Output emission of the sample was collected with a 10× Mitutoyo Plan APO infinity corrected objective (NA = 0.28) and coupled to a 750 mm spectrometer (Princeton Instruments SP2750) equipped with an electron multiplying charge-coupled device (CCD) camera (Princeton Instruments ProEM 1024BX3). The emission was spectrally and in-plane wavevector resolved using a 1,200 grooves mm^{-1} grating and a slit width of 50 μm at the entrance of the spectrometer. To obtain the incident excitation density of the pump pulse, the average pump power was measured using a calibrated Si photodetector (Thorlabs-Det10/M) and an oscilloscope (Keysight DSOX3054T) for data acquisition. Accuracy verification of the power measurements was carried out by using two independent power meters: (1) Si photodiode power sensor (Thorlabs-S120VC) with a power meter console (Thorlabs-PM100D), and (2) thermal power sensor (Thorlabs-S302C) equipped with the power meter console (Thorlabs-PM100D). The energy of the seed beam was calibrated by using standard power meter measurements and additionally verified through a single-photon counting technique using a photon counting module (SPC-160, Becker & Hickl GmbH) and a single-photon avalanche Si photodiode (IDQ100), for details see Supplementary Section VII. All the measurements for Figs. 2 and 3 are carried out under the same incident pump fluence of P_{pump} = 80 μJ cm^{-2} ($P \approx 2P_{th}$) to minimize the noise level originating from pump power fluctuations and high nonlinearity of the sample above the threshold. Pump fluence dependencies in Fig. 1b as well as spectra in Fig. 2d and the contrast dependence in Fig. 3 are plotted for the ground polariton state integrated within ±0.2 μm^{-1}.

Polariton single-condensate realizations were investigated by means of a single-shot real-space imaging technique using the same pump conditions ($P \approx 2P_{th}$) with individual pulse control. The images were recorded by means of an electron multiplying CCD camera applying 100× electron-multiplying gain and operating in a single-frame acquisition mode. To reduce the contribution of non-condensed polariton density we filtered out the output emission above ±1 μm^{-1} in Fourier space. To reduce the noise originated from pump fluctuation we recorded only realizations that obey 2% of tolerance interval in incident pump energy. The energy of incident pump pulses for each condensate realization was recorded using a calibrated photodetector and an oscilloscope. Using this selection criterion we recorded the single-condensate realizations represented in Fig. 4a–e by seeding the ground state for 300 sequential pulses followed by seed beam off measurements that allow for 300 realizations of spontaneously built polariton condensates. The whole sequence was repeated three times for each seed pulse energy. The incident seed energy was stabilized at the level of 2% standard deviation. Statistical analysis and calculation of the single-realization contrast in Fig. 4a–e were carried out through processing of all 900 spontaneously built and 900 seeded condensate realizations for each seed energy.

Data availability

All data supporting this study are openly available from the University of Southampton repository at https://doi.org/10.5258/SOTON/D1374.

33. Scherf, U., Bohnen, A. & Müllen, K. Polyarylenes and poly(arylenevinylene)s, 9 The oxidized states of a (1,4-phenylene) ladder polymer. *Makromol. Chem.* **193**, 1127–1133 (1992).

Acknowledgements Authors acknowledge A. Putintsev for technical support. This work was supported by the Russian Science Foundation (RSF) grant no. 20-72-10145 and the UK's Engineering and Physical Sciences Research Council grant EP/M025330/1 on Hybrid Polaritonics. E.S.A. and V.Yu.Sh. thank the Foundation for the Advancement of Theoretical Physics and Mathematics Basis. Yu.E.L. acknowledges Basic Research Program at the National Research University HSE, D.U., F.S. and T.S. acknowledge support by QuantERA project RouTe (SNSF grant no. 20QT21 175389). P.G.L, D.U., T.S. and R.F.M. acknowledge support by European H2020-FETOPEN project POLLOC (Grant No. 899141).

Author contributions A.V.Z., A.V.B. and D.S. performed the experiments and analysed the data. D.U., F.S., T.S. and R.F.M. contributed to the design and fabrication of the organic microcavity. U.S. synthesized the organic material. V.Yu.Sh., E.S.A. and Yu.E.L. developed microscopic theory and carried out numerical simulations. A.V.Z. and P.G.L. designed and led the research. The manuscript was written through contributions from all authors. All authors have given approval to the final version of the manuscript.

Competing interests The authors declare no competing interests.

Additional information

Supplementary information The online version contains supplementary material available at https://doi.org/10.1038/s41586-021-03866-9.

Correspondence and requests for materials should be addressed to Anton V. Zasedatelev or Pavlos G. Lagoudakis.

Peer review information *Nature* thanks the anonymous reviewers for their contribution to the peer review of this work. Peer reviewer reports are available.